NASA/CR-1999-209515
ICASE Report No. 99-31

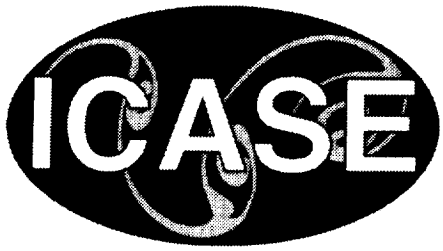

A Gas-kinetic Method for Hyperbolic-elliptic Equations and Its Application in Two-phase Fluid Flow

Kun Xu
ICASE, Hampton, Virginia
and
The Hong Kong University of Science & Technology, Hong Kong

Institute for Computer Applications in Science and Engineering
NASA Langley Research Center
Hampton, VA

Operated by Universities Space Research Association

National Aeronautics and
Space Administration

Langley Research Center
Hampton, Virginia 23681-2199

Prepared for Langley Research Center
under Contract NAS1-97046

August 1999

Available from the following:

NASA Center for AeroSpace Information (CASI)
7121 Standard Drive
Hanover, MD 21076-1320
(301) 621-0390

National Technical Information Service (NTIS)
5285 Port Royal Road
Springfield, VA 22161-2171
(703) 487-4650

A GAS-KINETIC METHOD FOR HYPERBOLIC-ELLIPTIC EQUATIONS AND ITS APPLICATION IN TWO-PHASE FLUID FLOW

KUN XU*

Abstract. A gas-kinetic method for the hyperbolic-elliptic equations is presented in this paper. In the mixed type system, the co-existence and the phase transition between liquid and gas are described by the van der Waals-type equation of state (EOS). Due to the unstable mechanism for a fluid in the elliptic region, interface between the liquid and gas can be kept sharp through the condensation and evaporation process to remove the "averaged" numerical fluid away from the elliptic region, and the interface thickness depends on the numerical diffusion and stiffness of the phase change. A few examples are presented in this paper for both phase transition and multifluid interface problems.

Key words. van der Waals equation of state, phase transition, interface capturing, kinetic scheme

Subject classification. Applied Numerical Mathematics

1. Introduction. The study of the liquid-gas phase transition and the interface movement have both theoretical and practical interesting. The macroscopic governing equations for this phenomena are the mixed hyperbolic elliptic system, where the van der Waals-type equation of state is usually used. Many numerical schemes have been proposed to solve the mixed type system, and the intensive investigation for the possible Riemann solver of the mixed type equations is still undergoing [24, 23, 6, 22, 5, 12, 14, 8]. Many criteria, such as viscosity capillarity and entropy rate admissibility conditions, have been well recognized in the capturing of realizable solutions.

Physically, the van der Waals model can be rigorously derived from statistical mechanics, and the coexistence region of liquid and gas can be well predicted from the Maxwell construction. The particle interaction with nearby repulsion and long ranged attraction can naturally give the phase transition and surface tension properties [16, 7]. Based on the particle interaction pictures, many Lattice Boltzmann schemes have been developed, see [20, 21, 26, 9, 17, 3] and refences therein, and the particle interaction mechanism is used to capture both multifluid interface and phase transition process. Recently, combining the macroscopic van der Waals equation of state (EOS) and the mesoscopic Lattice Boltzmann method, He et. al. developed an interesting scheme for the capturing of liquid and gas interface and they successfully applied the scheme to the study of the Rayleigh-Taylor instability [10]. However, the scheme in [10] only applies the van der Waals EOS to the index function and it does not capture the liquid and gas phase change. Also, the densities of the liquid and gas in [10] are artificially assigned which may not be consistent with the values from the van der Waals EOS and the Maxwell construction. Based on different interface sharpening mechanism, such as the reinitialization in the level set method, many interface capturing schemes have been developed in the past years, see [25, 13, 15] and references therein.

In this paper, we are going to develop a gas-kinetic BGK-type scheme for the hyperbolic elliptic system,

*Institute for Computer Applications in Science and Engineering, Mail Stop 132C, NASA Langley Research Center, Hampton, VA 23681-2199 (email: kxu@icase.edu) and Mathematics Department, The Hong Kong University of Science & Technology, Hong Kong (email: makxu@uxmail.ust.hk). This research was supported by the National Aeronautics and Space Administration under NASA Contract No. NAS1-97046 while the author was in residence at the Institute for Computer Applications in Science and Engineering (ICASE), NASA Langley Research Center, Hampton, VA 23681-2199. Additional support was provided by Hong Kong Research Grant Council through DAG98/99.SC22.

where the continuum and momentum equations are solved directly. The phase transition and the motion of multifluid interface are accurately captured by the current method.

2. Governing Equations and Interface Capturing Mechanism. In the one-dimensional case, the governing equations for the isothermal hyperbolic-elliptic system are

$$\begin{pmatrix} \rho \\ \rho U \end{pmatrix}_t + \begin{pmatrix} \rho U \\ \rho U^2 + p \end{pmatrix}_x = 0 \tag{2.1}$$

where ρ and U are the density and velocity. For the multiphase flow and phase transition problems, the relation between the pressure p and the density proposed by van der Waals is quite satisfactory. The equation of state is

$$p = \frac{\rho RT}{1 - b\rho} - a\rho^2,$$

where R is the gas constant, T is the temperature, and a and b are constants. The critical temperature for the separation of liquid and gas is

$$T_c = \frac{8a}{27bR}.$$

When the fluid temperature is below the above critical value, phase segregation occurs. In this paper, we are going to study the fluids with fixed values $a = 0.9$, $b = 0.25$ and $RT = 1.0$. The corresponding critical temperature in this case is $T_c = 1.0666/R$. Since RT is less than T_cR, the phase transition can appear in the current fluid system. The illustrative plot of the van der Waals EOS is shown in Fig.(5.1). The densities of liquid ρ_l and gas ρ_g can be obtained from Maxwell construction (equal area construction). The values in the plot are $1/\rho_l = 0.494273, 1/\rho_g = 1.405065, 1/\rho_\alpha = 0.574912, 1/\rho_\beta = 1.036251$. The fluid density ρ can be catalogued in the following regions:

$$\frac{1}{\rho} = \begin{cases} \frac{1}{\rho} < \frac{1}{\rho_l}, & \text{liquid phase} \\ \frac{1}{\rho_l} < \frac{1}{\rho} < \frac{1}{\rho_\alpha}, & \text{metastable} \\ \frac{1}{\rho_\alpha} < \frac{1}{\rho} < \frac{1}{\rho_\beta}, & \text{unstable elliptic region (mixture)} \\ \frac{1}{\rho_\beta} < \frac{1}{\rho} < \frac{1}{\rho_g}, & \text{metastable} \\ \frac{1}{\rho_g} < \frac{1}{\rho}, & \text{gas phase} \end{cases} \tag{2.2}$$

When the fluid density takes on values in the elliptical region, due to the negative slope of $\partial p/\partial \rho$, fluid instabilities will be amplified. The fluid mixture in the elliptic region will evaporate to the gas state or condense to the liquid state. So, similar to the shock steepening mechanism, the van der Waals EOS has an intrinsic physical mechanism to separate different phases at the multifluid interface and sharpen the interface. This is the main reason that we can observe the sharp liquid gas interface in the real world. This property can also be used to develop an interface capturing scheme.

Numerically, due to the cell size limitation and averaging process [28], the liquid and gas will be artificially mixed to form a numerical mixture with averaged density. If there is no any steepening mechanism at the interface, such as at the contact discontinuity wave of the compressible Euler equations, the thickness of the interface will grow with the square root of evolution time or total number of time steps. The real sharp interface between different fluids is enforced through the van der Waals-type EOS or the molecular interactions. Once this kind of physics is incorporated in a multifluid numerical scheme, the numerically averaged density in the elliptical region will be condensed to the liquid or evaporated to the gas and the numerical interface can be kept sharp automatically.

In order to use the steepening mechanism at a multifluid interface, a scheme must be very accurate in predicting the liquid and gas densities first. In other words, even though there is no explicit terms about Maxwell equal area construction in Eq.(2.1), a scheme must have certain intrinsic dissipative mechanism, such as the implicit viscosity capillarity terms, and be able to pick up the physically correct solutions, such as the same liquid and gas densities from the Maxwell construction. Then, a numerically averaged density can be most likely located in the elliptic region. On the other hand, the numerical diffusion cannot be too large or it will overtake the physical steepening mechanism in the elliptic region.

Currently, it seems difficult for any high-order scheme to predict a very accurate density jump at a multifluid interface. It is not surprising that many existing high-order schemes will give liquid and gas densities which probably depend on the interpolation limiters, CFL number, the cell size, even the Runge-Kutta time stepping techniques. In the current paper, we present a gas-kinetic scheme to solve Eq.(2.1). Due to the intrinsic diffusion and dissipative mechanism in the kinetic approach [28], the Maxwell equal area rule is implicitly achieved. The numerically obtained equilibrium densities of liquid and gas are very close to the theoretical values. At the same time, the phase boundary can be kept within two or three grid points. With this property, the kinetic method is used to simulate the evolution of multifluid interface, such as the merging of two liquid droplets.

3. Gas-Kinetic Scheme for the Hyperbolic-Elliptic Equations. The BGK model has the standard form

$$f_t + uf_x = \frac{g - f}{\tau}, \tag{3.1}$$

where f is the gas distribution function, g is the equilibrium state, and τ is the particle collision time. Both f and g are functions of space x, time t, and particle velocity u.

In order to recover Eq.(2.1) from Eq.(3.1), the equilibrium state g can be constructed as

$$g = \rho(\frac{\lambda}{\pi})^{\frac{1}{2}} e^{-\lambda(u-U)^2},$$

where λ is defined by

$$\begin{aligned} \lambda &= \frac{\rho}{2p} \\ &= \frac{1}{2}\frac{1 - b\rho}{RT - a\rho + ab\rho^2} \\ &= \Lambda(\rho), \end{aligned} \tag{3.2}$$

and the variation of λ is related to the density changes

$$\begin{aligned} d\lambda &= \frac{1}{2}\frac{ab^2\rho^2 - 2ab\rho + (a - bRT)}{(RT - a\rho + ab\rho^2)^2} d\rho \\ &= D(\rho)d\rho, \end{aligned} \tag{3.3}$$

where the functions Λ and D are well defined in the above equations. In the current paper, a fixed value $RT = 1.0$ is used.

Due to the conservation properties in particle collision, f and g satisfy the compatibility condition

$$\int (f - g)\psi_\alpha du = 0 \qquad \text{for} \qquad \psi_\alpha = (1, u)^T \tag{3.4}$$

at any point in space and time.

The solution for the BGK model (3.1) is

$$f(x_{j+1/2},t,u)=\frac{1}{\tau}\int_0^t g(x',t',u)e^{-(t-t')/\tau}dt'+e^{-t/\tau}f_0(x_{j+1/2}-ut), \tag{3.5}$$

where $x_{j+1/2}$ is the cell interface and $x'=x_{j+1/2}-u(t-t')$ is the particle trajectory. There are two unknowns in the above equation. One is the initial gas distribution function f_0 at time $t=0$, and the other is g in both space and time locally around $(x_{j+1/2},t=0)$. Similar to the BGK-type schemes for the Euler and Navier-Stokes equations [28], the numerical scheme based on Eq.(3.5), along with the compatibility condition (3.4), is described as follows:

Step(1): Use MUSCL technique [27] to interpolate the conservative variables $W=(\rho,\rho U)^T$, and obtain the reconstructed initial data inside each cell

$$W_j(x)=W_j(x_j)+\frac{W_j(x_{j+1/2})-W_j(x_{j-1/2})}{x_{j+1/2}-x_{j-1/2}}(x-x_j)\quad \text{for}\quad x\in[x_{j-1/2},x_{j+1/2}], \tag{3.6}$$

where $W_j(x_j)$ is the cell averaged value, and $W_j(x_{j-1/2})$ and $W_j(x_{j+1/2})$ are the values at the cell boundaries. A nonlinear limiter, such as van Leer's limiter, is used in the current paper to get the cell boundary values. From the reconstructed data, the values ρ,U and their corresponding slopes, e.g. $\partial\rho/\partial x$ and $\partial U/\partial x$, are known everywhere. Therefore, the variation λ can be found subsequently through Eq.(3.3), such as $\partial\lambda/\partial x=D(\rho)\partial\rho/\partial x$.

Step(2): Based on the reconstructed data in Step(1), around each cell interface $x_{j+1/2}$, construct the initial gas distribution function f_0,

$$f_0(x)=\begin{cases} g^l\left(1+a^l(x-x_{j+1/2})\right), & x\le x_{j+1/2}\\ g^r\left(1+a^r(x-x_{j+1/2})\right), & x\ge x_{j+1/2}, \end{cases} \tag{3.7}$$

where the states g^l and g^r are the Maxwellian distribution functions defined in terms of the conservative variables at a cell interface,

$$g^l=g^l(W_j(x_{j+1/2}))\qquad\text{and}\qquad g^r=g^r(W_{j+1}(x_{j+1/2})). \tag{3.8}$$

For example, with the distribution

$$g^l=\rho^l(\frac{\lambda^l}{\pi})^{\frac{1}{2}}e^{-\lambda^l(u-U^l)^2}, \tag{3.9}$$

all coefficients in g^l can be obtained as

$$\begin{pmatrix}\rho^l\\ U^l\\ \lambda^l\end{pmatrix}=\begin{pmatrix}\rho_j(x_{j+1/2})\\ \rho_jU_j(x_{j+1/2})/\rho_j(x_{j+1/2})\\ \Lambda(\rho^l)\end{pmatrix}. \tag{3.10}$$

Similar formulation can be found for g^r. The coefficients $a^{l,r}$ in Eq.(3.7) have the forms

$$a^{l,r}=m_1^{l,r}+m_2^{l,r}u+m_3^{l,r}u^2,$$

which are derived from the Taylor expansion of a Maxwellian distribution function. The coefficients $(m_1^{l,r},\ m_2^{l,r},\ m_3^{l,r})$ depend on (ρ^l,U^l), (ρ^r,U^r) and their corresponding slopes, *i.e.*

$$\left(\frac{\partial\rho^l}{\partial x},\frac{\partial U^l}{\partial x},\frac{\partial\lambda^l}{\partial x}\right)\qquad\text{and}\qquad\left(\frac{\partial\rho^r}{\partial x},\frac{\partial U^r}{\partial x},\frac{\partial\lambda^r}{\partial x}\right).$$

The detail relations are

$$
\begin{aligned}
m_1^{l,r} &= \left[\frac{1}{\rho}\left(\frac{\partial \rho}{\partial x}\right) + (\frac{1}{2\lambda} - U^2)\frac{\partial \lambda}{\partial x} - 2\lambda U \frac{\partial U}{\partial x}\right]^{l,r}, \\
m_2^{l,r} &= \left[2U\frac{\partial \lambda}{\partial x} + 2\lambda \frac{\partial U}{\partial x}\right]^{l,r}, \\
m_3^{l,r} &= \left[-\frac{\partial \lambda}{\partial x}\right]^{l,r}.
\end{aligned} \tag{3.11}
$$

Therefore, with the initially reconstructed data in Step (1), $f_0(x)$ in Eq.(3.7) are totally determined. For the sake of simplicity, we assume $x_{j+1/2} = 0$ in the rest of this paper.

Step(3): The equilibrium state g is constructed as

$$
g = g_0\left(1 + (1 - \mathrm{H}[x])\bar{a}^l x + \mathrm{H}[x]\bar{a}^r x + \bar{A}t\right), \tag{3.12}
$$

where $\mathrm{H}[x]$ is the Heaviside function and g_0 is the state located at $(x = 0, t = 0)$,

$$
g_0 = \rho_0(\frac{\lambda_0}{\pi})^{\frac{1}{2}} e^{-\lambda_0(u-U_0)^2}. \tag{3.13}
$$

The coefficients $\bar{a}^l, \bar{a}^r$, and $\bar{A}$ in Eq.(3.12) have the forms

$$
\begin{aligned}
\bar{a}^{l,r} &= \bar{m}_1^{l,r} + \bar{m}_2^{l,r} u + \bar{m}_3^{l,r} u^2, \\
\bar{A} &= \bar{A}_1 + \bar{A}_2 u + \bar{A}_3 u^2,
\end{aligned} \tag{3.14}
$$

which have the same functional dependence on $(\partial\rho/\partial x, \partial U/\partial x)$ and $(\partial\rho/\partial t, \partial U/\partial t)$, as shown in Eq.(3.12).

Taking both limits $(x \to 0)$ and $(t \to 0)$ in Eq.(3.5) and (3.12), and applying the compatibility condition at $(x = 0, t = 0)$, we can get macroscopic quantities W_0,

$$
W_0 = \begin{pmatrix} \rho_0 \\ \rho_0 U_0 \end{pmatrix} = \int g_0 \psi_\alpha du = \int \left(g^l \mathrm{H}[u] + g^r(1 - \mathrm{H}[u])\right)\psi_\alpha du, \tag{3.15}
$$

where g^l and g^r are known from Step (2). Here W_0 is the "averaged" flow variables at the cell interface, from which g_0 can be determined. Then, connecting W_0 to the cell centered values $W_j(x_j)$ and $W_{j+1}(x_{j+1})$, we can get the slopes for mass and momentum distributions on both sides

$$
\begin{aligned}
\left(\frac{\partial \rho_0^l}{\partial x}, \frac{\partial(\rho_0 U_0)^l}{\partial x}\right)^T &= \frac{W_0 - W_j(x_j)}{x_{j+1/2} - x_j} \qquad \text{for} \qquad x \le 0, \\
\left(\frac{\partial \rho_0^r}{\partial x}, \frac{\partial(\rho_0 U_0)^r}{\partial x}\right)^T &= \frac{W_{j+1}(x_{j+1}) - W_0}{x_{j+1} - x_{j+1/2}} \qquad \text{for} \qquad x \ge 0,
\end{aligned} \tag{3.16}
$$

from which $\partial\rho/\partial x, \partial U/\partial x, \partial\lambda/\partial x$ can be obtained. Therefore, $(\bar{a}^l, \bar{a}^r)$ can be determined in a similar way as that in Eq.(3.12). The only unknown in Eq.(3.12) is $\bar{A}$, which is related to $\partial\rho_0/\partial t$, $\partial U_0/\partial t$ and $\partial\lambda_0/\partial t$ $(= D(\rho_0)\partial\rho_0/\partial t)$ through the relations

$$
\begin{aligned}
\bar{A}_1 &= \left[\frac{1}{\rho_0}\left(\frac{\partial \rho_0}{\partial t}\right) + (\frac{1}{2\lambda_0} - U_0^2)\frac{\partial \lambda_0}{\partial t} - 2\lambda_0 U_0 \frac{\partial U_0}{\partial t}\right]^{l,r}, \\
\bar{A}_2 &= \left[2U_0\frac{\partial \lambda_0}{\partial x} + 2\lambda_0 \frac{\partial U_0}{\partial t}\right]^{l,r}, \\
\bar{A}_3 &= \left[-\frac{\partial \lambda_0}{\partial t}\right]^{l,r}.
\end{aligned} \tag{3.17}
$$

To this point, we need to evaluate $\partial\rho_0/\partial t$ and $\partial(\rho U)_0/\partial t$.

Step(4): Substituting Eqs.(3.12) and (3.7) into the integral solution (3.5), we obtain the distribution function f at $x = 0$,

$$\begin{aligned} f(0,t,u) = \gamma_0 g_0 + \gamma_1 \left(\bar{a}^l \mathrm{H}[u] + \bar{a}^r(1-\mathrm{H}[u])\right) u g_0 \\ +\gamma_2 \bar{A} g_0 + \gamma_3 \left((1-uta^l)\mathrm{H}[u]g^l + (1-uta^r)(1-\mathrm{H}[u])g^r\right), \end{aligned} \tag{3.18}$$

where

$$\begin{aligned} \gamma_0 &= 1 - e^{-t/\tau}, \\ \gamma_1 &= \tau(-1 + e^{-t/\tau}) + te^{-t/\tau}, \\ \gamma_2 &= \tau(t/\tau - 1 + e^{-t/\tau}), \\ \gamma_3 &= e^{-t/\tau}. \end{aligned}$$

The only unknown in Eq.(3.18) is $\bar{A}$, which is a function of $(\partial\rho_0/\partial t, \partial U_0/\partial t)$, see Eq.(3.18). Since the compatibility condition must be satisfied everywhere in space and time, it can be integrated in a whole CFL time step ΔT at $x = 0$

$$\int_0^{\Delta T} \int \left(f(0,t,u) - g(0,t,u)\right) \psi_\alpha dt du = 0, \tag{3.19}$$

from which

$$\begin{aligned} (\Gamma_5 \frac{\partial \rho_0}{\partial t}, \Gamma_5 \frac{\partial(\rho U)_0}{\partial t})^T = \int \left[-\Gamma_3 g_0 + \Gamma_1 u \left(\bar{a}^l \mathrm{H}[u] + \bar{a}^r(1-\mathrm{H}[u])\right) g_0\right. \\ + \Gamma_3 \left(\mathrm{H}[u]g^l + (1-\mathrm{H}[u])g^r\right) \\ \left. + \Gamma_4 u \left(a^l \mathrm{H}[u]g^l + a^r(1-\mathrm{H}[u])g^r\right)\right] \psi_\alpha du \end{aligned} \tag{3.20}$$

are obtained. All terms on the right hand side of the above equation are known, and

$$\begin{aligned} \Gamma_0 &= \Delta T - \tau(1 - e^{-\Delta T/\tau}), \\ \Gamma_1 &= \tau\left(-\Delta T + 2\tau(1 - e^{-\Delta T/\tau}) - \Delta T e^{-\Delta T/\tau}\right), \\ \Gamma_2 &= \frac{1}{2}\Delta T^2 - \tau\Delta T + \tau^2(1 - e^{-\Delta T/\tau}), \\ \Gamma_3 &= \tau(1 - e^{-\Delta T/\tau}), \\ \Gamma_4 &= -\tau\left(-\Delta T e^{-\Delta T/\tau} + \tau(1 - e^{-\Delta T/\tau})\right), \\ \Gamma_5 &= \tau\left(\Delta T - \tau(1 - e^{-\Delta T/\tau})\right). \end{aligned}$$

Thus, $(\partial\rho_0/\partial t, \partial U_0/\partial t)$, as wel as $\partial\lambda_0/\partial t$, can be obtained from Eq.(3.21).

Step(5): The time-dependent numerical fluxes of mass and momentum across the cell interface is

$$F_{W,j+1/2} = \begin{pmatrix} F_\rho(t) \\ F_{\rho U}(t) \end{pmatrix}_{j+1/2} = \int u\psi_\alpha f_{j+1/2}(0,t,u) du, \tag{3.21}$$

where f is given in Eq.(3.18). The update of flow variables inside each cell becomes

$$W_j^{n+1} = W_j^n + \frac{1}{\Delta x}\int_0^{\Delta t} (F_{W,j-1/2} - F_{W,j+1/2}) dt.$$

4. Numerical Examples. In this section, we are going to present a few test cases in both 1D and 2D. The van Leer limiter is used for interpolations of ρ and ρU at the beginning of each time step. The time step ΔT is determined by the Courant-Friedrichs-Levy condition with CFL number =0.25. The collision time τ is defined as

$$\tau = C_1 \Delta T + C_2 \Delta T \frac{|p^l - p^r|}{p^l + p^r}, \tag{4.1}$$

where $p^l = \Lambda(\rho^l)$, $p^r = \Lambda(\rho^r)$, and $C_1 = 0.05, C_2 = 2.0$ are fixed in all calculations.

4.1. 1D Shock Tube Cases. In the following, four shock tube cases presented in Shu's paper [22] are tested using the current kinetic scheme.

CASE(1)

The initial condition for this case is the exact liquid and gas densities from the Maxwell construction,

$$(1/\rho_L = 0.494273, U_L = 1.0)|_{x<0.5} \qquad \text{and} \qquad (1/\rho_R = 1.405065, U_R = 1.0)|_{x\geq 0.5}.$$

The cell size used is $\Delta x = 1/200$. This test case is mainly to see if the scheme can keep the admissible jump from the Maxwell construction. The numerical result (solid line and circles) for the density distribution is shown in Fig.(5.2), where the dashed and dotted lines represent $1/\rho_l, 1/\rho_g, 1/\rho_\alpha$ and $1/\rho_\beta$ respectively.

CASE(2)

The second case has the following initial condition,

$$(1/\rho_L = 0.54, U_L = 1.0) \qquad \text{and} \qquad (1/\rho_R = 1.8517, U_R = 1.0).$$

This initial jump satisfies the Rankine-Hugoniot condition, but does not satisfy the physical principles, such as viscosity capillarity condition. With the cell size $\Delta x = 1/200$, our simulation results are shown in Fig.(5.3), where the solid line is obtained with a much refined mesh $\Delta x = 1/2000$. This case clearly shows that the current scheme can pick up the physically admissible solution. There is no oscillations at the liquid phase around the interface. Our results are favorable in comparison with the ENO-type method [22].

CASE(3)

This case has the initial condition

$$(1/\rho_L = 0.45, U_L = 1.0) \qquad \text{and} \qquad (1/\rho_R = 2.0, U_R = 2.0).$$

Fig.(5.4) shows the results with cell sizes $\Delta x = 1/200$ and $\Delta x = 1/2000$. From this figure, we can also observe the sharp interface between the liquid and gas phases.

CASE(4)

The initial condition for this case is

$$(1/\rho, U) = (0.8 + 0.2\sin(x), 1 - 0.5\cos(x)).$$

The initial density is entirely in the elliptic region. Periodic boundary condition is used. The solutions with cell size $\Delta x = 1/400$ at different output time are shown in Fig.(5.5). These figures clearly show the flow instability in the elliptic region and how the densities eventually go to the well defined liquid and gas densities, even though the Maxwell construction is not explicitly used in the current scheme. For the liquid and gas phases, the numerical densities obtained are about $1/\rho = (0.49400, 1.40175)$. The differences between the numerics and the theoretical values $(0.494273, 1.405065)$ are less than 0.5%. This is a very good case to test the ability of any high-order scheme to capture the correct density jumps around the phase boundary, as well as the sharpness of the interface. Our scheme can capture the jump within 2 or 3 cells, as shown in Fig(5.5d).

4.2. Liquid-Gas Interfaces in 2D Cases. In 2D cases, in order to capture the movement of a multifluid interface the inclusion of surface tension and gravity becomes important. In the test case (5), the gravitational force ρG is implemented in the y-momentum equation for the liquid phase, and the nondimensional magnitude of G is assigned the value 0.25. In the test case (6), an additional body force $\kappa\rho\nabla\nabla^2\rho$ is added in the momentum equations to recover the surface tension effect [19, 3, 10]. The nondimensional coefficient κ used in case (6) is equal to 5.0×10^{-6}.

CASE(5)

This is a dam break problem. Many schemes have been used in this kind of free surface problems. A short list includes Volume of Fluid (VOF), Boundary Integral Techniques, Front Tracking Method, and Arbitrary Lagrangian-Eulerian (ALE) method, see [11, 29, 4, 1] and references therein. The cell size used in our study is $\Delta x = \Delta y = 1/100$. The schematic construction for this problem is shown in Fig.(5.6), where the densities of the liquid and gas are assigned with the values from the Maxwell construction, i.e. $1/\rho_l = 0.494273$ and $1/\rho_g = 1.405065$. The initial velocity of both gas and liquid are zero, and no surface tension is included in this case. Due to the numerical diffusion, any index function to describe the liquid and gas interface will get smeared in the Eulerian advection scheme, and the smearing is proportional to the square root of the number of time steps used. This is basically the main reason for the level set method to use reinitialization to keep the interface sharp [2]. However, in our case, since the van der Waals EOS is used to describe the liquid and gas phases, any smeared density at the interface is most likely to locate in the elliptic region and the flow instability in these region will automatically steepen the interface. More specifically, the condensation and evaporation process around phase boundary could move the averaged density to the liquid or gas phases, and this effect compensates the numerical dissipation in the advection scheme. Fig.(5.7) shows the time evolution of the liquid-gas interface, and the interface thickness keeps two or three mesh size regardless the time steps used to get the final results. Fig.(5.8) shows the locations of the leading liquid front. The numerical results are compared with the experimental data in [18]. From this figure, we observe that the numerical speed is slower than the experimental speed. The reason for the difference is that in the current calculation the density ratio between liquid and gas is about 2.8, and the experimental data was obtained for the water and air, and their density ratio is about 800. Therefore, the relative aerodynamical resistence is much higher in the current study. Fig.(5.7) shows a very interesting phenomena that there is a bore shock and a rarefaction wave in the liquid phase. This solution is amazingly close to the solution by solving the shallow water equations. In other words, the current direct numerical simulation in some sense validates the approximation used in theoretical derivation of shallow water equations.

CASE(6)

This test case is about the collision of two droplets. Similar to the last case, the initial densities of the liquid and gas phases are assigned with the theoretical values again from the Maxwell construction, *i.e.* $1/\rho_l = 0.494273$ and $1/\rho_g = 1.405065$. The cell size used in this case is $\Delta x = \Delta y = 1/100$. The initial droplets with radius $R = 0.055$ are moving toward each other with a velocity magnitude of $U = 0.125$. No gravity is included in this case. Fig.(5.9) shows the time evolution of the droplets. The collision and merging of the droplets can be observed. Due to the steepening mechanism at the fluid interfaces from the van der Waals EOS, the sharp interface is kept in the time evolution process. Fig.(5.10) shows the density distribution across the central lines in both the x- and the y-directions of Fig.(5.9i), where the phase boundaries keep 2 mesh points even though 1600 time steps have passed at that output time.

5. Discussion and Conclusion. In this paper, we have developed a gas-kinetic scheme for the hyperbolic-elliptic system, where the van der Waals equation of state is used to describe the phase transition.

At the same time, the instability or sharpening mechanism in the elliptical region is used to capture the fluid interface. Many test cases validate the current approach.

The current paper is only a first step in the study of multifluid flow by solving the mixed type system. Hopefully, in the near future we can answer the following questions.

1. If we only need to describe the motion of multifluid interfaces without including phase transition, such as problems related to incompressible multifluid, we need to find some ways to simplify the van der Waals EOS in order to get a simple (not simpler) numerical method. But, the property $\partial p/\partial \rho < 0$ has to be kept so as to get the interface sharpening mechanism.

2. The current approach can be used to capture the interface breaking and merging. Similar to the level set method, the interface topological changes is easily handled. However, since the equations are basically describing the phase transition problems, the mass conservation for each individual phase cannot be guaranteed in the evolution process. How to improve the mass conservation property for each individual phase under the current framework is an important question that needs to be addressed.

3. In order to increase the density ratio between the liquid and gas phases, we need to use a more realistic EOS to cope with that.

The preliminary results presented in this paper are very promising and encouraging. Since there is no tracking, index function, or special treatment used around the multifluid interfaces, the extension of the current method to simulate hundreds or even thousands of bubbles (or droplets) becomes possible. Also, the implementation of interface physics in the capturing of interface movement should be a reasonable and reliable approach. This kind of scheme may provide a new way to solve many multifluid engineering problems after its further developement.

Acknowledgments. We would like to thank X.Y. He and L.S. Luo for helpful discussions about phase transition and multiphase flow problems, and thank M. Salas for his reviewing of the current paper and valuable advices.

REFERENCES

[1] R.K. Chan, *A Generalized Arbitrary Lagrangian-Eulerian Method for Incompressible Flows with Sharp Interfaces*, J. Comput. Phys., **58** (1975), pp. 311-331.

[2] Y.C. Chang, T.Y. Hou, B. Merriman, and S. Osher, *A Level Set Formulation of Eulerian Interface Capturing Methods for Incompressible Fluid Flows*, J. Comput. Phys., **124** (1996), pp. 449-464.

[3] Y. Chen, S. Teng, T. Shukuwa, and H. Ohashi, *Lattice-Boltzmann Simulation of Two-phase Fluid Flows*, Int. J. Modern Physics C, **9** (1998), pp. 1383-1391.

[4] I.L. Chern, J. Glimm, O. McBryan, B. Plohr, and S. Yaniv, *Front Tracking for Gas Dynamics*, J. Comput. Phys., **62** (1986), pp. 83-110.

[5] B. Cockburn and H. Gau, *A Model Numerical Scheme for the Propagation of Phase Transitions in Solids*, SIAM J. Sci. Comp., **17** (1996), pp. 1092-1121.

[6] H. Fan, *Traveling Waves, Riemann Problems and Computations of a Model of the Dynamics of Liquid/Vapor Phase Transitions*, J. Diff. Eqn., **150** (1998), pp. 385-437.

[7] N.G. Hadjiconstantinou, A. Garcia, and B.J. Alder, *The Surface Properties of a van der Waals Fluid*, submitted to Phys. Rev. Lett. (1999).

[8] H. Hattori, *The Riemann Problem of a System for a Phase Transition Problem*, International Series of Numerical Mathematics, **129** (1999), pp. 455-464.

[9] X. He, X. Shan and G.D. Doolen, *A Discrete Boltzmann Equation Model for Nonideal Gases*, Phys. Rev. E, **57** (1998), pp. R13.

[10] X.Y. He, S.Y. Chen, and R.Y. Zhang, *A Lattice Boltzmann Scheme for Incompressible Multiphase Flow and Its Application in Simulation of Rayleigh-Taylor Instability*, J. Comput. Phys., **152** (1999), pp. 642-663.

[11] C.W. Hirt and B.D. Nichols, *Volume of Fluid (VOF) Method for the Dynamics of Free Boundaries*, J. Comput. Phys., **39** (1981), pp. 201-225.

[12] D.Y. HSIEH AND X.P. WANG, *Phase Transition in van der Waals Fluid*, SIAM J. Appl. Math., **57** (1997), pp. 871-892.

[13] R. ISSA AND O. UBBINK, *Numerical Prediction of Taylor Bubble Dynamics Using A New Interface Capturing Technique*, Proceedings of the 3rd ASME/JSME Joint Fluid Engineering Conference, FEDSM99-7103 (1999).

[14] S. JIN, *Numerical Integrations of Systems of Conservation Laws of Mixed Type*, SIAM J. Appl. Math., **55** (1995), pp. 1536-1551.

[15] F.J. KELECY AND R.H. PLETCHER, *The Development of a Free Surface Capturing Approach for Multidimensional Free Surface Flows in Closed Containers*, J. Comput. Phys., **138** (1997), pp. 939-980.

[16] J.L. LEBOWITZ AND O. PENROSE, *Unified Theory of Lattice Boltzmann Model for Nonideal Gases*, J. Math. Phys., **7** (1966), pp. 98.

[17] L. LUO, *Unified Theory of Lattice Boltzmann Model for Nonideal Gases*, Physical. Review Letters, **81** (1998), pp. 1618-1621.

[18] J.C. MARTIN AND W.J. MOYCE, *An Experimental Study of the Collapse of Liquid Columns on a Horizontal Plane*, Philos. Trans. R. Soc. Lond. A, **244** (1952), pp. 312-324.

[19] B.T. NADIGA AND S. ZALESKI, *Investigation of a Two-phase Fluid Model*, Eur. J. Mech. B/Fluids, **15** (1996), pp. 885.

[20] D.H. ROTHMAN AND S. ZALESKI, *Lattice-gas Models of Phase separation: Interface, Phase Transitions and Multiphase Flow*, Rev. Mod. Ohys., **66** (1994), pp. 1417.

[21] X. SHAN AND H. CHEN, *Simulation of Non-ideal Gases and Liquid-gas Phase Transitions by the Lattice Boltzmann Equation*, Phys. Rev. E, **49** (1994), pp. 2941.

[22] C.W. SHU, *A Numerical Method for Systems of Conservation Laws of Mixed Type Admitting Hyperbolic Flux Splitting*, J. Comput. Phys., **100** (1992), pp. 424-429.

[23] M. SLEMROD AND J.E. FLAHERTY, *Numerical Investigation of a Riemann Problem for a van der Waals Fluids*, Phase Transformation, C.A. Elias and G. John, eds., Elsevier, New York (1986).

[24] H.B. STEWART AND B. WENDROFF, *Two-phase Flow: Models and Methods*, J. Comput. Phys., **56** (1984), pp. 363-409.

[25] M. SUSSMAN, P. SMEREKA, AND S. OSHER, *A Level Set Approach for Computing Solutions to Incompressible Two-phase Flow*, J. Comput. Phys., **114** (1994), pp. 146-159.

[26] M.R. SWIFT, W.R. OSBORN, AND J.M. YEOMANS, *Lattice Boltzmann Simulation of Nonideal Fluids*, Phys. Rev. Lett., **75** (1995), pp. 830.

[27] B. VAN LEER, *Towards the Ultimate Conservative Difference Scheme IV, A New Approach to Numerical Convection*, J. Comput. Phys., **23** (1977), pp. 276.

[28] K. XU, *Gas-kinetic Schemes for Compressible Flow Simulations*, 29th CFD lecture series 1998-03, Von Karman Institute (1998).

[29] R.W. YEUNG, *Numerical Methods in Free Surface Flows*, Ann. Rev. Fluid Mech., **14** (1982), pp. 395.

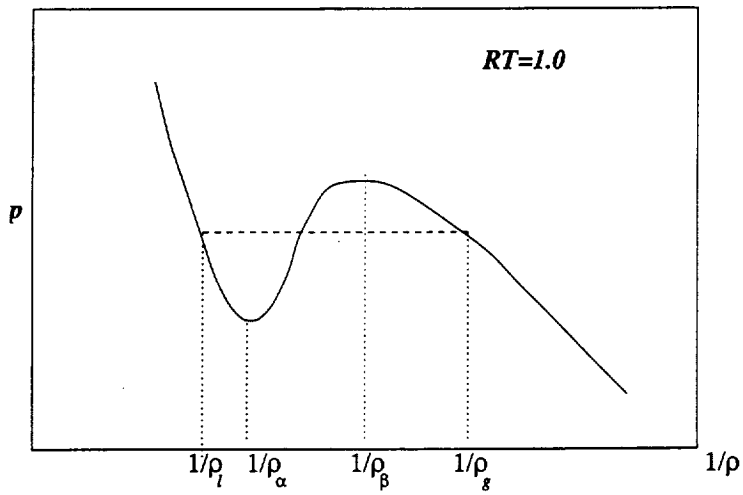

FIG. 5.1. *van der Waals Equation of State for* $RT = 1.0$ *case.*

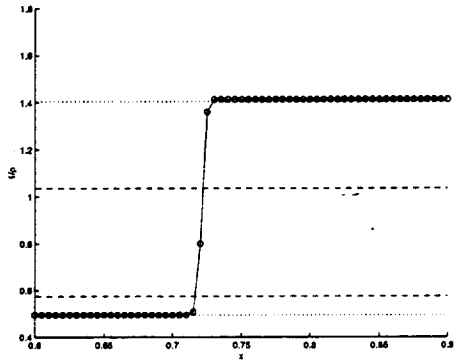

FIG. 5.2. *Solid line and circles are the distribution of* $1/\rho$. *The dotted lines are densities of* $1/\rho_l$ *and* $1/\rho_g$ *from Maxwell construction. The region between dashed lines* $(1/\rho_\alpha, 1/\rho_\beta)$ *is the elliptic region where the fluid is intrinsically unstable.*

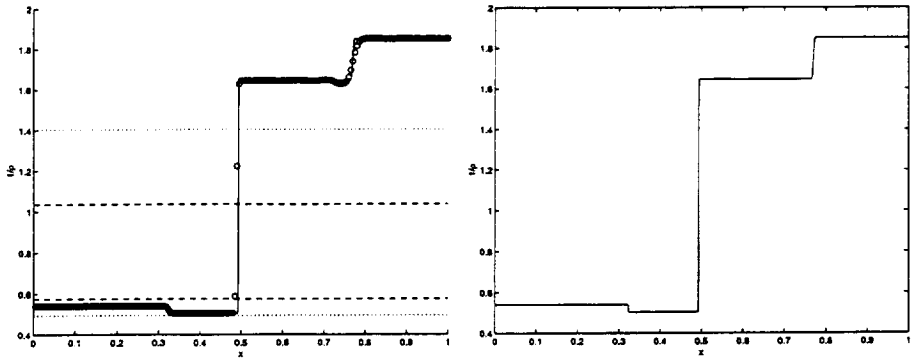

FIG. 5.3. *(a) Circles are the simulation results of distribution* $1/\rho$, *which are obtained with the cell size* $\Delta x = 1/200$. *The solid line is the result obtained with a much refined mesh* $\Delta x = 1/2000$. *(b) Distribution of* $1/\rho$ *obtained with a refined mesh* $\Delta x = 1/2000$.

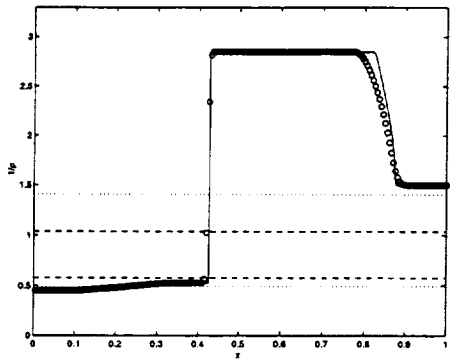

FIG. 5.4. *Distribution of $1/\rho$. Circles are the simulation result obtained with cell size $\Delta x = 1/200$. The solid line is the result obtained with a much refined mesh $\Delta x = 1/2000$.*

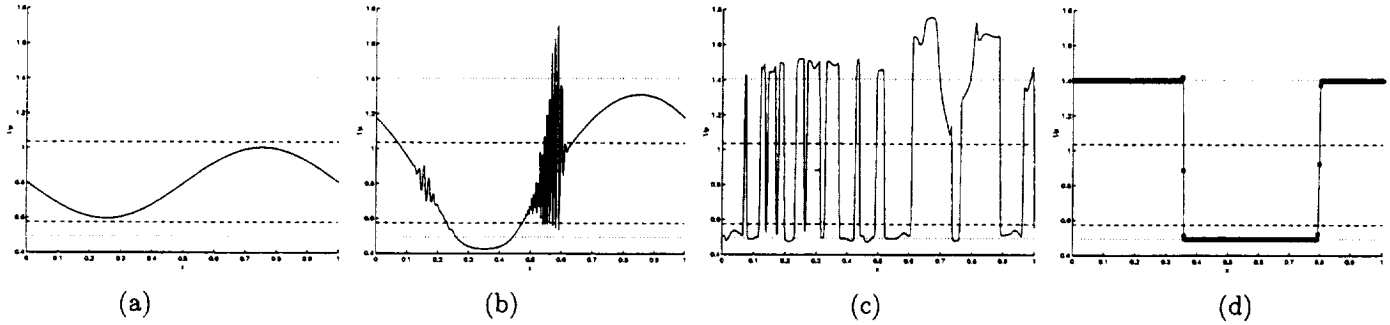

FIG. 5.5. *The solid lines are the distributions of $1/\rho$ at different output times. The mesh size used is $\Delta x = 1/400$. (a) t=0.0, (b) t=0.1, (c) t=1.0, (d) t=100.0. Circles are added in the plot (d) to show the number of grid points around the multifluid interfaces.*

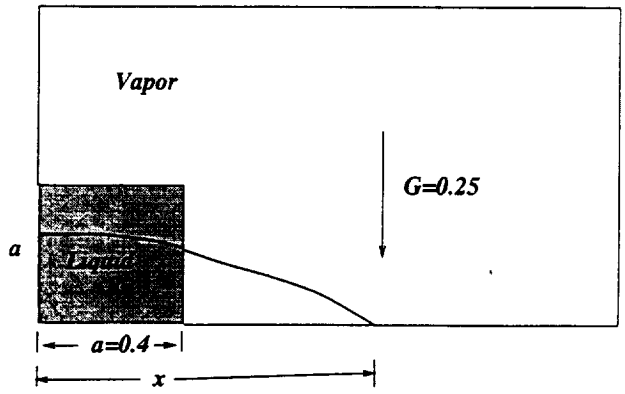

FIG. 5.6. *Schematic diagram of liquid gas distributions.*

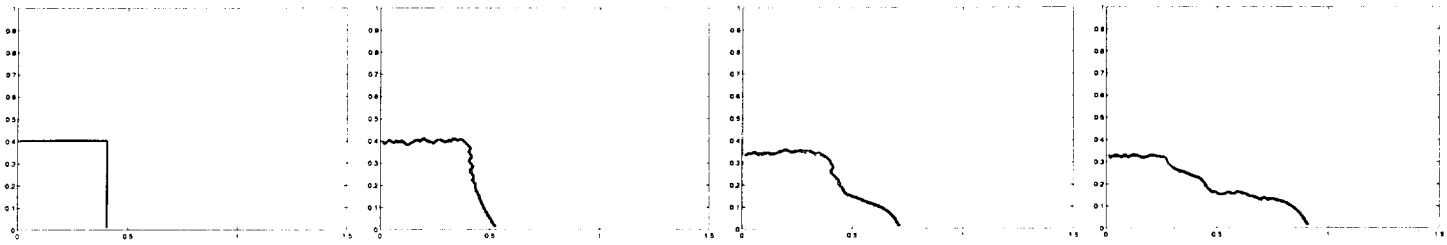

(a) (b) (c) (d)

FIG. 5.7. *Liquid-gas interfaces at different output time. (a)* $t = 0.0$, *(b)* $t\sqrt{G/a} = 0.5$, *(c)* $t\sqrt{G/a} = 1.0$, *(d)* $t\sqrt{G/a} = 1.5$.

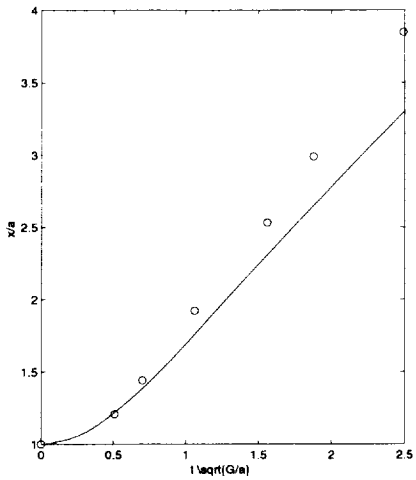

FIG. 5.8. *The horizontal axis is* $t\sqrt{G/a}$ *and the vertical axis is* x/a, *where* x *is the location of leading liquid front. The solid line is the time evolution of the leading liquid front. The density ratio between liquid and gas is around* 2.8. *The circle is the experimental data in [18], where real water and air with density ratio around* 800 *were used.*

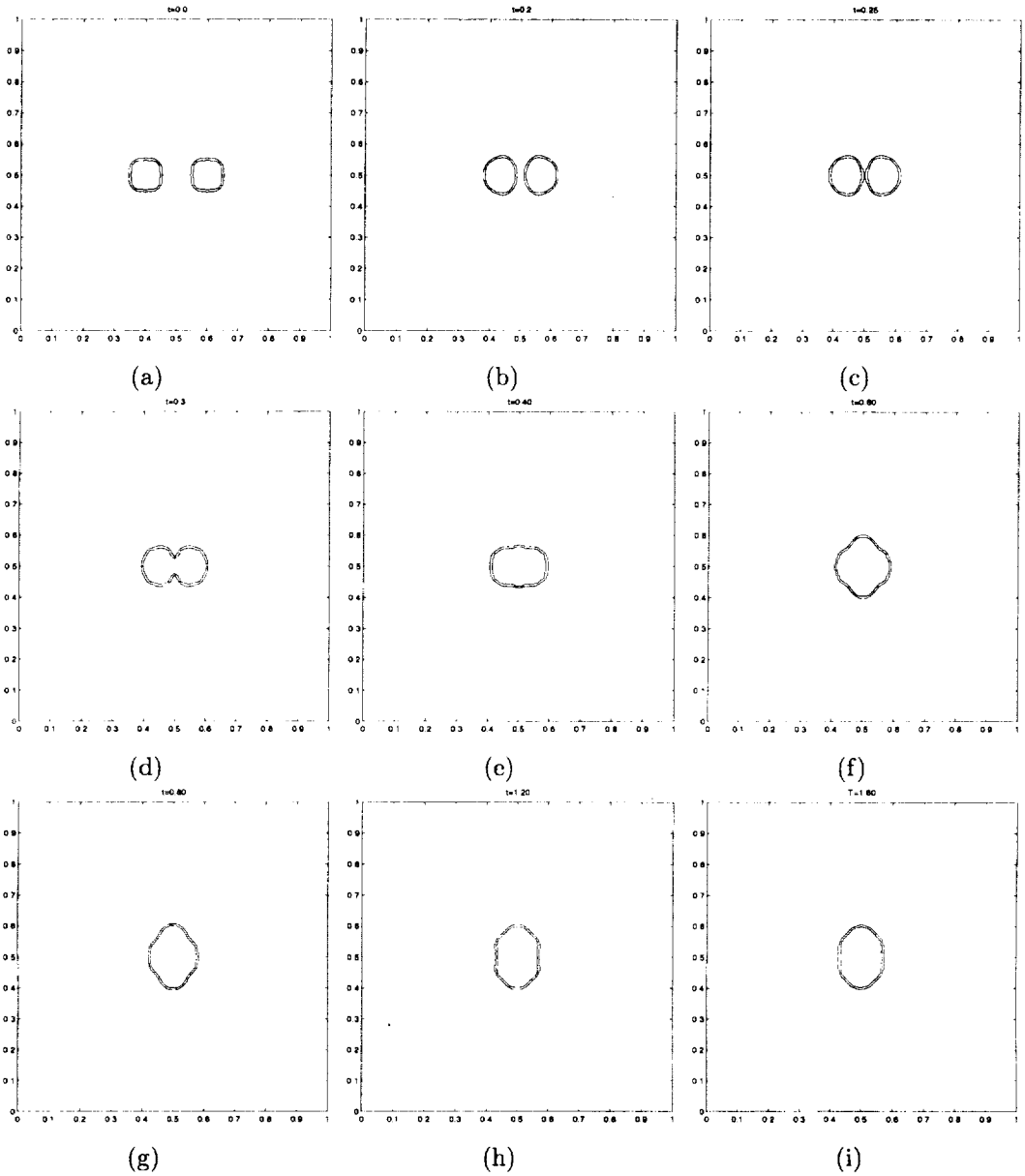

FIG. 5.9. *Time evolution of the collision of two droplets. The output times are (a) t=0, (b) t=0.2, (c) t=0.25, (d) t=0.3, (e) t=0.40, (f) t=0.60, (g) t=0.80, (h) t=1.20, (i) t=1.60.*

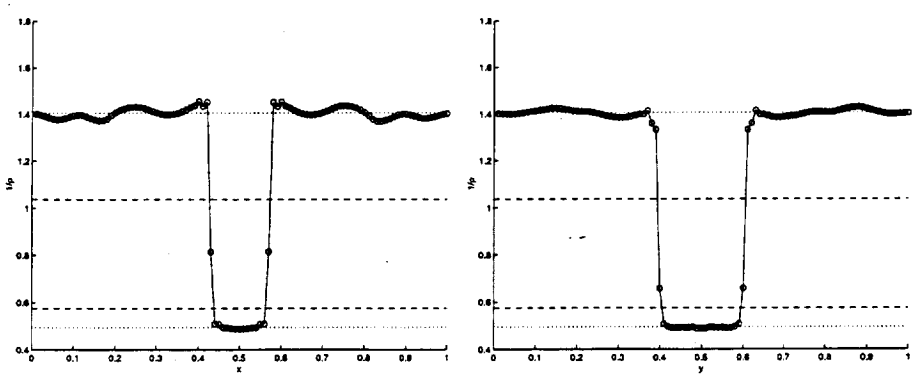

FIG. 5.10. *The distribution $1/\rho$. (a). along the central line of Fig.(5.9i) in the x-direction, (b). along the central line of Fig.(5.9i) in the y-direction. Since both the liquid and gas are treated as the compressible flow in the current study, small density fluctuations appear in the dynamical transport process, especially in the gas phase.*

REPORT DOCUMENTATION PAGE

Form Approved
OMB No. 0704-0188

1. AGENCY USE ONLY *(Leave blank)*	2. REPORT DATE	3. REPORT TYPE AND DATES COVERED
	August 1999	Contractor Report

4. TITLE AND SUBTITLE
A gas-kinetic method for hyperbolic-elliptic equations and its application in two-phase fluid flow

5. FUNDING NUMBERS
C NAS1-97046
WU 505-90-52-01

6. AUTHOR(S)
Kun Xu

7. PERFORMING ORGANIZATION NAME(S) AND ADDRESS(ES)
Institute for Computer Applications in Science and Engineering
Mail Stop 132C, NASA Langley Research Center
Hampton, VA 23681-2199

8. PERFORMING ORGANIZATION REPORT NUMBER
ICASE Report No. 99-31

9. SPONSORING/MONITORING AGENCY NAME(S) AND ADDRESS(ES)
National Aeronautics and Space Administration
Langley Research Center
Hampton, VA 23681-2199

10. SPONSORING/MONITORING AGENCY REPORT NUMBER
NASA/CR-1999-209515
ICASE Report No. 99-31

11. SUPPLEMENTARY NOTES
Langley Technical Monitor: Dennis M. Bushnell
Final Report
To be submitted to SIAM Journal of Scientific Computing.

12a. DISTRIBUTION/AVAILABILITY STATEMENT
Unclassified Unlimited
Subject Category 64
Distribution: Nonstandard
Availability: NASA-CASI (301) 621-0390

12b. DISTRIBUTION CODE

13. ABSTRACT *(Maximum 200 words)*
A gas-kinetic method for the hyperbolic-elliptic equations is presented in this paper. In the mixed type system, the co-existence and the phase transition between liquid and gas are described by the van der Waals-type equation of state (EOS). Due to the unstable mechanism for a fluid in the elliptic region, interface between the liquid and gas can be kept sharp through the condensation and evaporation process to remove the "averaged" numerical fluid away from the elliptic region, and the interface thickness depends on the numerical diffusion and stiffness of the phase change. A few examples are presented in this paper for both phase transition and multifluid interface problems.

14. SUBJECT TERMS
van der Waals equation of state, phase transition, interface capturing, kinetic scheme

15. NUMBER OF PAGES
20

16. PRICE CODE
A03

17. SECURITY CLASSIFICATION OF REPORT	18. SECURITY CLASSIFICATION OF THIS PAGE	19. SECURITY CLASSIFICATION OF ABSTRACT	20. LIMITATION OF ABSTRACT
Unclassified	Unclassified		

NSN 7540-01-280-5500

Standard Form 298(Rev. 2-89)
Prescribed by ANSI Std. Z39-18
298-102